energies

MDPI

Article

Liquid vs. Gas Phase CO_2 Photoreduction Process: Which Is the Effect of the Reaction Medium?

Alberto Olivo [1], Elena Ghedini [1], Michela Signoretto [1,*], Matteo Compagnoni [2] and Ilenia Rossetti [2]

[1] CatMat Lab, Department of Molecular Sciences and Nanosystems, Ca' Foscari University Venice and Consortium INSTM, RU of Venice, Via Torino 155, 30172 Venezia, Italy; alberto.olivo@unive.it (A.O.); gelena@unive.it (E.G.)

[2] Chemical Plants and Industrial Chemistry Group, Department of Chemistry, Università Degli Studi di Milano, Consortium INSTM, RU of Milano Università and CNR-ISTM, via C. Golgi 19, 20133 Milan, Italy; matteo.compagnoni@unimi.it (M.C.); ilenia.rossetti@unimi.it (I.R.)

* Correspondence: miky@unive.it; Tel.: +39-041-234-8650

Received: 2 August 2017; Accepted: 7 September 2017; Published: 13 September 2017

Abstract: The use of carbon dioxide, the most concerning environmental issue of the 21st century, as a feedstock for fuels productions still represents an innovative, yet challenging, task for the scientific community. CO_2 photoreduction processes have the potential to transform this hazardous pollutant into important products for the energy industry (e.g., methane and methanol) employing a photocatalyst and light as the only energy input. In order to design an effective process, the high sustainability of this reaction should be matched with the perfect reaction conditions to allow the reactant, photocatalyst, and light source to come together: therefore, the choice of reaction conditions, and in particular its medium, is a crucial issue that needs to be investigated. Throughout this paper, a careful study of carbon dioxide photoreduction in liquid and vapour phases are reported, focusing on their effect on catalyst performances in terms of light harvesting, productivity, and selectivity. Different from most papers in the literature, catalytic tests were performed under extremely low light irradiance, in order to minimise the primary energy input, highlighting that this experimental variable has a great effect on the reaction pathway and, thus, product distribution.

Keywords: CO_2 photoreduction; reaction medium; titanium dioxide; liquid phase; gas phase; product distribution

1. Introduction

Nowadays carbon dioxide emissions represent one of the most threatening issues to the environment due to its considerable contribution to several phenomena, such as the increase in global temperatures in recent centuries [1]. The correlation between increasing CO_2 emissions and the use of fossil fuels has been undoubtedly established, but none of the actions put in place seems effective to harness CO_2 emissions [2,3].

Several strategies can be pursued to mitigate carbon dioxide emissions into the atmosphere and their effects [4–6]: though geologic or oceanic storage are already applied to this purpose [7–9], the transformation into valuable or highly-requested products is conceptually more favourable [10]. A very attractive strategy is the conversion of carbon dioxide into fuels, which might lead to a real circular economy, avoiding the use of net CO_2-producing energy sources. In this way, the product of hydrocarbon combustion, i.e., water and carbon dioxide, are converted into regenerated fuels in a process that was labelled by some authors as artificial photosynthesis [11–14].

Over the years, CO_2 photocatalytic reduction attracted attention, since it is able to reach this goal using a light source as the primary energy input which, in the foreseeable future, might be possibly

obtained from the sun [15,16]. The presence of a photocatalyst and its physicochemical properties are essential to the development of a robust and reliable process. At the moment, several semiconductors have been employed (such as ZnO, ZnS, WO_3, Fe_2O_3, ZrO_2 [17–20]), but titanium dioxide-based materials are the most promising due to large availability, low cost, and the appropriate band-gap for this application [21,22].

Despite great effort on the development of an efficient photocatalyst, the choice of the optimal reaction conditions is not a secondary issue. Due to the novelty of this technology and the flourishing of publications on this topic, different rig configurations are reported in the literature. Since the first study by Inoue and co-workers [23], liquid phase systems have been widely developed. Water use, both as reagent and solvent, has been deeply investigated due to its great availability, inexpensiveness, and environmental friendliness. However, water as a solvent for this reaction suffers from a low carbon dioxide solubility [24,25], which hinders the possibility for CO_2 to interact with the catalyst dispersed in the reaction medium. To overcome this drawback, several strategies have been pursued over the years.

The substitution of water with organic solvents, such as methanol [26], isopropanol [27], or acetonitrile, proved to be effective to increase carbon dioxide solubility and, thus, photoactivity, despite a negative effect on the economic and environmental sustainability of the process. Another possibility is the use of alkali solutions as reaction media [28–30]. In this case, carbon dioxide is dissolved as bicarbonate ions which are more stable in the aqueous medium but, unfortunately, are characterised by a higher reduction potential, further limiting process efficiency [31].

An alternative possible and most promising strategy is to boost the reaction conditions, which has been previously studied by some of the authors [32]. Indeed, the increase of pressure allows enhancing carbon dioxide uptake in the liquid reaction medium, so as to increase reduction products and overall process productivity.

In the last decade, vapour phase reactors became popular over time [33–36], thanks to an easier reactant mixing, which leads to the possibility to tune the CO_2/H_2O ratio and also to perform this reaction under CO_2 excess [37], enhancing in this way carbon dioxide adsorption on the catalytic surface [38]. As a matter of fact, Tahir and Amin showed that reagent ratio productivity and product selectivity to methane is maximised for a 1.5 CO_2/H_2O ratio, which is above the stoichiometric 0.5 value [39].

Carbon dioxide adsorption aside, light harvesting should be carefully considered because of the lower refractive index of gases when compared to water (1.000464 for CO_2, 1.34795 and 1.000256 for liquid and vapour water, respectively, at 293 K, 361 nm light wavelength [40,41]). A variety of geometries has been brought up for photoreactors, aimed at maximising catalyst photoactivation. In the liquid phase, most commonly-used systems are featured by a quartz window that allows light to enter [42–44]. More recently, some papers in the literature reported the use of an annular design that allows a homogeneous light transfer to the catalyst, mainly in the radial direction [32,45].

Generally, energy input is represented by UV light and irradiance, a metric for energy input, is usually in the range of 1000–3000 $W \cdot m^{-2}$, which is extremely higher than UV light fraction in sunlight [15,46–48]. Very few papers report results from tests performed at lower irrandiances: for example, Woolerton and co-workers performed CO_2 photoreduction tests in the aqueous phase using UVA 450 $W \cdot m^{-2}$ irradiance [49], while, more recently Tahir et al. reported results at 200 $W \cdot m^{-2}$ in the vapour phase conditions [50]. However, to the best of our knowledge, papers reporting CO_2 photoreduction tests using an irradiance below 100 $W \cdot m^{-2}$ have not been published yet, except for previous papers from the authors [32,39]. The promising performances even at low irradiance conditions is an important step towards the use of the most sustainable and inexpensive light source, i.e., sunlight.

From this overview, it is clear that reaction conditions, and in particular the reaction medium, affect catalyst effectiveness in light harvesting and reactant interaction with it, thus playing a crucial role. Moreover, in literature a wide variety of photocatalysts and photoreactors have been reviewed

but the reaction medium effect on catalytic performance is still not clear and, to the best of the author's knowledge, this topic has not been experimentally investigated yet. Therefore, the goal of the work is the assessment of experimental conditions for CO_2 photoreduction. In particular, titanium dioxide-based materials were tested both in the liquid and vapour phases for a direct comparison under extremely-low irradiance conditions to understand the reaction medium effect on process efficiency.

2. Results and Discussion

2.1. Materials Characterisation

For the purposes of this work, two commercial titanium dioxide-based materials were chosen to compare their photocatalytic performances with a lab-made titanium dioxide sample. Thus, a preliminary characterisation was performed to assure material suitability for photocatalytic application.

As shown in the N_2 physisorption isotherms (Figure 1), all three samples show a type-IV isotherm typical of mesoporous materials.

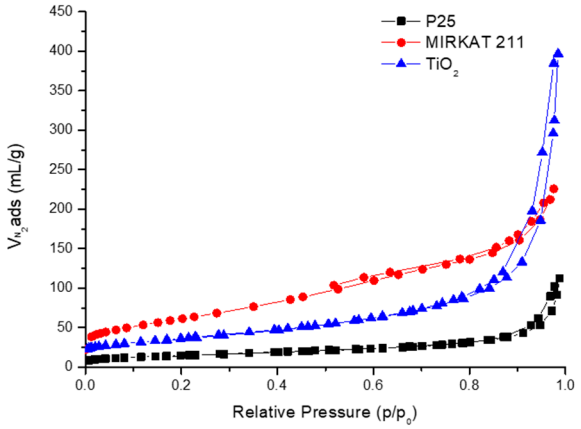

Figure 1. P25, MIRKAT 211, and TiO_2 N_2 physisorption isotherms.

P25, which is the most commonly used benchmark material [51], provides the lowest surface area (50 $m^2 \cdot g^{-1}$) and the isotherm shows a narrow hysteresis loop at high relative pressures (between 0.8 and 1 p/p_0), indicating a narrow distribution of pores with an average pore size of 15 nm. The lab-made sample (labelled as TiO_2) shows a similar isotherm in shape, but a greater nitrogen adsorption, indicating a higher surface area. As a matter of fact, TiO_2 has a 110 $m^2 \cdot g^{-1}$, which is double that of P25, and an average pore size of 25 nm, whereas MIRKAT 211 is characterised by a much higher surface area (217 $m^2 \cdot g^{-1}$) and is characterized by a higher nitrogen adsorption at low relative pressures and a wider hysteresis loop, corresponding to a wider and non-homogeneous pore size distribution.

Considering the materials' crystal structures, there are some differences among the three samples, as shown by X-ray diffraction (XRD) diffractograms reported in Figure 2.

In MIRKAT 211 and the TiO_2 sample, the only observed crystal phase is anatase, in accordance with JCPDS card No. 00-002-0387; this structure is the most suitable crystal phase for photocatalytic applications, due to the highest electron-hole life among titanium dioxide polymorphs [52]. Moreover, due to the desired application for CO_2 photoreduction, the anatase conduction band is more reductive than the rutile band gap, thus, in principle, more suitable to reduce CO_2, which is a highly energy-demanding reaction [53,54].

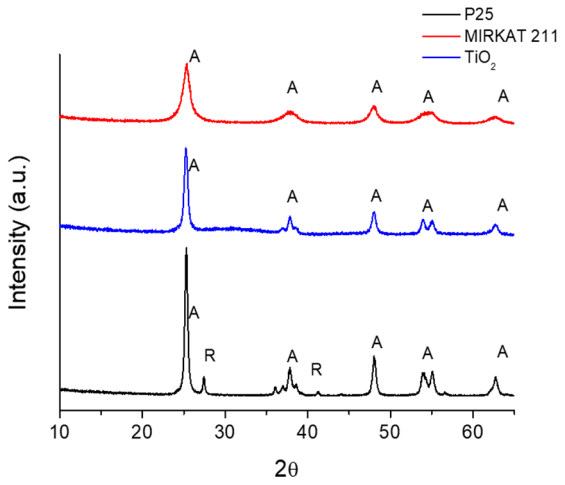

Figure 2. P25, MIRKAT 211, and TiO_2 XRD patterns. A represents the diffraction peaks of the anatase phase, R, those of the rutile phase.

Comparing the two profiles, the TiO_2 sample provides sharper and more defined peaks than MIRKAT 211, indicating a higher crystallinity in the former sample. As a matter of fact, the MIRKAT 211 manufacturer states that this product is made up of 40 wt % anatase, while the rest is amorphous TiO_2 [55,56]. Instead, according to Rietveld analysis, it is composed of 98 wt % anatase and the remaining part is amorphous. Conversely, P25 shows not only anatase-related peaks, but also diffraction peaks due to rutile (JCPDS card No. 76-1940). In fact, it is known that this material is made up of a mixture of the two crystal structures in a ca. 75/25 anatase/rutile ratio [57]. Despite rutile's fast electron-hole recombination, the co-presence of the anatase and rutile crystallites creates an electronic circulation from the photoexcited rutile lattice trapping sites, the most easily excitable, yet unstable, to anatase ones which are the most resistant to electron-hole recombination [58]. This feature is also observable in the diffuse reflectance spectroscopy (DRS) spectra reported in Figure 3 and is often correlated to the enhanced lifetime of the photogenerated charges.

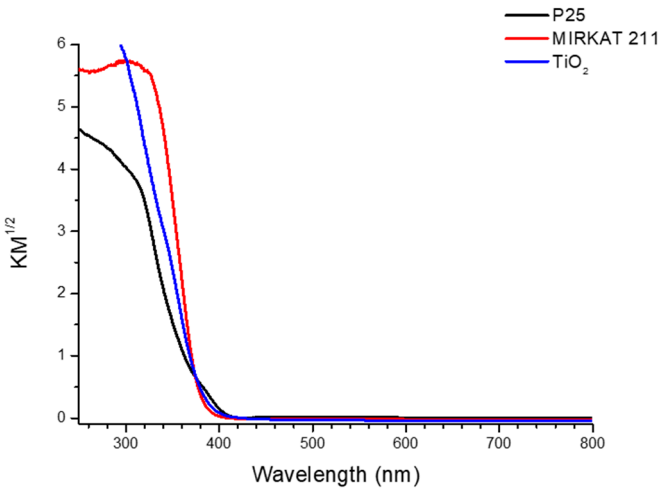

Figure 3. P25, MIRKAT 211, and TiO_2 DRS spectra.

MIRKAT 211 and the TiO_2 sample provide a typical sharp absorption below 390 nm, corresponding to a 3.2 eV band gap (typical of anatase), in accordance to the XRD patterns and data reported in the literature [59]. Differently, P25 provides a small absorption between 390 and 410 nm due to the small fraction of rutile and below 390 nm absorption due to anatase. Considering the

polymorph structure of this material, the P25 overall band gap is 3.1 eV, which is lower than the pure anatase titanium dioxide.

In conclusion, all materials are suitable, in principle, for CO_2 photoreduction despite their different morphological and structural properties. P25 differs in surface, crystal, and electronic properties from the other two samples, which are indeed characterised by a much higher surface area and anatase as the only crystal phase.

2.2. Vapour Phase Photocatalytic Results

Before performing the activity runs, blank tests were carried out in order to avoid any bias in data collection and interpretation. In fact, traces of organic species can definitely lead to misleading results [60]. In the case of our freshly-prepared sample, only inorganic salts were used in the preparation of the catalyst and residual sulphate ions were eliminated by washing. However, in order to check the presence of carbonaceous species possibly deriving from manipulation, the following tests were performed: without light, catalyst, or reactants. In none of the three cases we observed any hydrocarbon formation. Moreover, a test with catalyst, light, and water (so, without CO_2 only) was performed, and no C-based product was detected, indicating the absence of carbonaceous species on the surface. Thus, it is possible to state, first of all, that this reaction is not a photochemical reaction, but a photocatalytic one. Moreover, catalysts are photostable and do not contain any trace of carbon from their manipulation, and collected data are not affected by carbonaceous species on the photocatalytic surface.

Photocatalytic tests with these three samples in the vapour phase are reported in Figure 4. In both testing rigs, it was chosen to use low-irradiance conditions (i.e., 50 $W \cdot m^{-2}$) in order to minimise energy input and unequivocally determine and appreciate the differences in catalytic behaviours due to material morphology and experimental conditions. Such a low irradiance with respect to the literature reports is suggested by the useful energy fraction that can be reasonably exploited from solar light irradiation. In the case of bare titanium dioxide, radiation energy for a material excitation must be greater than, or at least equal to, its band gap (BG), i.e., 3.2 eV for anatase and 3.0 for rutile, which limit its application to UV irradiation. To increase VIS light absorption, TiO_2's BG is usually narrowed in the case of environmentally-benign photooxidations, but this usually leads to a decrease in conduction band's reductant properties. In fact, reduction potential for CO_2 is quite close to TiO_2's conduction band potential, strongly limiting band gap reduction strategies.

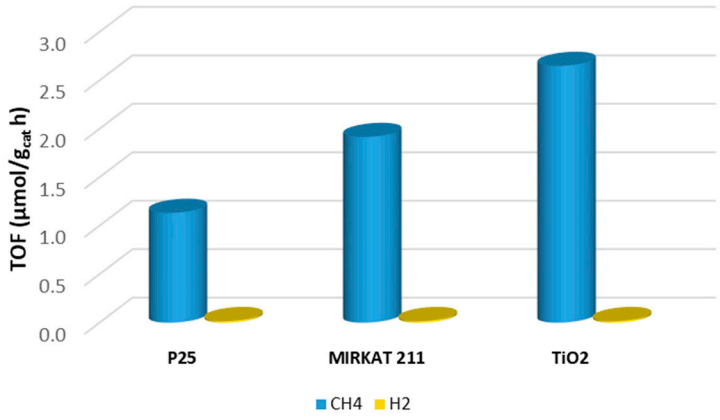

Figure 4. P25, MIRKAT 211, and TiO_2 photocatalytic tests in the vapour phase: methane and hydrogen productivities.

In vapour phase tests, the only detected products were methane and hydrogen. The former was the most abundant product with all three catalysts. Methane derives from complete carbon dioxide photoreduction and no trace of other carbonaceous species, like CO or formaldehyde, were detected.

Karamian and co-workers [61], reported that, in most cases, in gaseous systems CO is the first intermediate product of CO_2 photoreduction by water vapour. However, reaction conditions, and in particular temperature, irradiance, and reaction time, can modify the reaction pathway and, thus, product distribution. In particular, when CO_2 deoxygenation is faster than dehydrogenation, methane production is favoured with respect to oxygenated compounds [62]. This is the case of vapour phase reaction, characterised by CO_2 excess. This mechanism involves the formation of C radicals that recombine with H originated from water [63].

At the same time, hydrogen can be produced from water splitting into hydrogen and oxygen, which, in this case, can be potentially responsible for reductant consumption. In all cases, here, selectivity to methane was higher than 98%, indicating that CO_2 photoreduction is favoured with respect to water splitting.

Among the three samples, P25 is the least active material in methane production and this experimental evidence is ascribable to its lower surface area, which limits the number of available photocatalytic sites and adsorbed species. Conversely, MIRKAT 211, despite the highest surface area, provides lower methane production than the TiO_2 sample, which is the best performing material. This photocatalytic behaviour is ascribable to the co-presence of two favourable features, i.e., relatively high surface area and high crystallinity of the anatase phase, which seems to be more effective on photoactivity. Indeed, small crystals expose boundary defective sites that may act as electron-hole recombination centres, thus decreasing the photocatalytic activity. This means that, to increase TiO_2 efficiency in CO_2 photoreduction in the gas phase under low-irradiance conditions it is necessary to formulate materials characterised by high surface area and high crystallinity in the anatase phase at the same time.

2.3. Liquid Phase Photocatalytic Results

In this case, blank tests were performed preliminarily. No evidence of activity under dark conditions or in the absence of catalyst or CO_2 was observed, indicating that carbon reactants, catalyst, and light are necessary for the reaction to proceed and that there are not any residual carbonaceous species from sample manipulation. Water splitting was not significant in this case, mainly based on the selection of the hole scavenger and operating conditions.

Considering the liquid phase activity results, no methane was detected for all three samples. However, differently from the vapour phase systems, higher amounts of hydrogen and C-containing products in the liquid phase (methanol, formic acid, formaldehyde) were detected. This was expected, since the mechanism of photoreduction is completely different in liquid or gas-phase system [64]. A recent investigation on the reaction mechanism and product distribution vs. time, showed that liquid phase products accumulate as primary species in the liquid phase, followed by parallel and consecutive reactions. Among these, hydrogen and CO are produced by photoreforming of the newly-reduced organic compounds. Furthermore, in similar photocatalytic systems [61,65,66], it is reported that the reaction is triggered by the formation of peroxocarbonate species, which are reduced to formic acid, formaldehyde, and methanol afterwards. Due to the higher H_2O/CO_2 ratio, it is plausible that $\cdot CO_2^-$ undergoes hydrogenation faster than deoxygenation, leading to all those products found in the liquid phase. However, as reported by Liu and Li [62], hydroperoxo species in water are characterised by a high redox potential, which makes them very unstable and, thus, unreliably detectable. Therefore, we can speculate that in our conditions the unstable peroxocarbonates are the first intermediates, then directly converted into formate ions, formic acid, and further reduction products.

If CO_2 is absorbed in water at neutral pH (molecular form), it is consecutively reduced to formic acid, formaldehyde, and methanol. Formaldehyde is, instead, the first forming product when basic aqueous solutions are adopted, and further reduction to methanol or oxidation to formic acid may occur. Hydrogen and CO/CO_2 form in the gas phase, but their formation reaction is consecutive to the accumulation of organic compounds in the liquid phase and the depletion of Na_2SO_3, used as a

hole scavenger [67]. Indeed, after sulphite consumption, the formed organic compounds start acting as hole scavengers in a photoreforming reaction scheme.

When testing the present samples, we observed hydrogen as a predominant product in the gas phase, with increasing concentration passing from P25 (negligible), to MIRKAT 211, and to TiO_2. Carbon monoxide was detected only for MIRKAT and TiO_2 in very small amounts compared to hydrogen (1% of the total gas phase products for both the materials). This indicates high selectivity to the full reoxidation to CO_2 of the organic compounds in the photoreforming step.

Additionally, the best outcomes, in terms of C-containing products, were obtained using sample TiO_2, essentially for the same reasons outlined in the previous paragraph. Figure 5 shows the results in terms of TOF. Furthermore, P25 revealed the worst activity, due to a lower surface area, in spite of the slightly lower band gap.

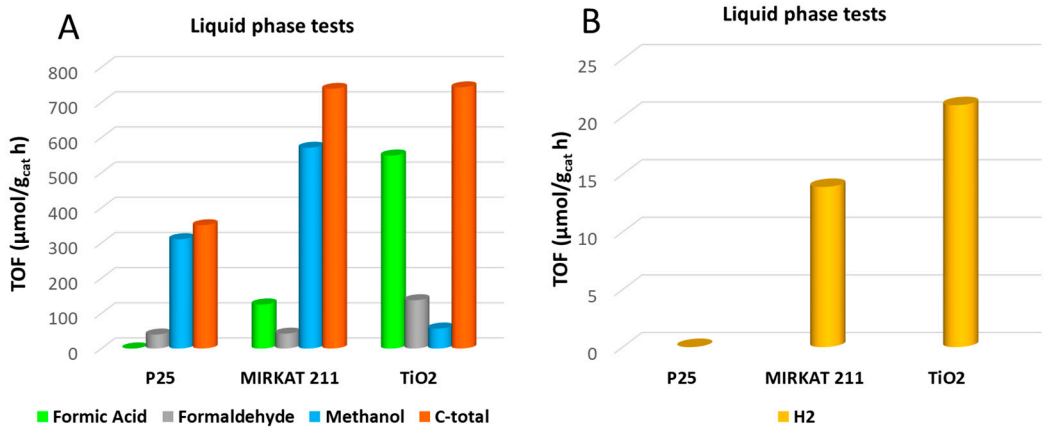

Figure 5. P25, MIRKAT 211, and TiO_2 photocatalytic tests in liquid phase: (**A**) liquid phase C-containing compounds; and (**B**) hydrogen productivities.

Similar productivities of the liquid phase products were obtained for the TiO_2 and the MIRKAT 211 samples, which is ca. double with respect to the P25 sample, and much higher than the CH_4 amount achieved in the gas phase testing rig. This is explained, in part, considering the higher reduction potential needed for the reduction from CO_2 to CH_4 than to obtain partially-reduced compounds. On the other hand, this demonstrates the better performance achievable with liquid-phase CO_2 photoreduction, provided that improved solubility is reached using relatively high pressure testing. The product distribution in the liquid phase, considering P25 and MIRKAT 211, are in accordance with the consecutive reaction steps occurring at neutral pH [64]. Indeed, the higher concentration of methanol is detected, being the final product formed during the CO_2 photoreduction process. However, the product distribution in the case of sample TiO_2 was different, since a maximum concentration was obtained for formic acid, with total C formed in the liquid phase being comparable with MIRKAT 211 and ca. double that of P25. The highest H_2 productivity, and the lowest of methanol, are interpreted on the basis of a higher turnover rate, which depletes the sulphite hole scavenger faster, with consequently faster start-up of the oxidation of the organic products through photoreforming.

2.4. Effect of Reaction Medium

In both experimental conditions, despite surface area being important, crystallinity and suitable crystal phase (i.e., anatase) represent the most important physicochemical properties for an efficient TiO_2 photocatalyst. The choice of performing under equal and extremely low irradiance allows the even greater appreciation of these differences in the effectiveness of the different materials in light harvesting and, thus, in carbon dioxide conversion.

Results in vapour and liquid phase tests are directly compared here, which has never been done before from an experimental point of view. The tests have been carried out under specifically-optimised

conditions for both testing modes. It is clear that process activity and selectivity is driven by the reaction medium. From all experimental evidence, it is possible to suppose that a reduction in the titanium dioxide valence band undergoes two different pathways, as shown in Figure 6. In one case, fast deoxygenation leads to C species that are reduced afterwards whereas, in the liquid phase, hydroperoxo species undergo hydrogenation preferentially [68], yielding to possible intermediate products. The liquid phase product distribution of sample TiO_2 confirms the proposed mechanism (74% formic acid, 18% formaldehyde, 8% methanol).

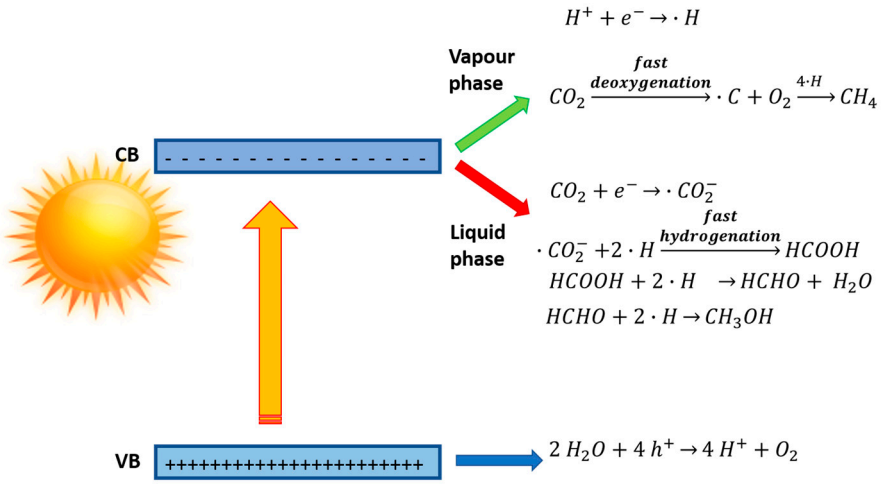

Figure 6. Different reaction mechanisms in vapour and liquid phases.

Therefore, different reaction pathways are active when operating in the two different media, which led to direct production of the most reduced product (methane) in the gas phase system whereas, in the liquid phase, intermediate reduction products are formed together with H_2.

As for testing in the liquid phase, it should be remarked that the key for significant productivity is related to the possibility to achieve sufficiently high CO_2 solubility in water by applying a sufficiently high pressure.

3. Materials and Methods

3.1. Materials

The following reagents were used as received: $TiOSO_4 \cdot xH_2O \cdot yH_2SO_4$ (Ti assay > 29% Sigma Aldrich, Milan, Italy), sodium hydroxide (assay > 97% Carlo Erba, Milan, Italy), and 2-propanol (assay 99.8% Fluka, Milan, Italy). Two standard TiO_2 reference materials were used. The first one is the most commonly used titanium dioxide, i.e., P25 from Degussa (Essen, Germany), used as a reference for comparison with the literature. The second one is MIRKAT 211, which has been purchased by Euro Support s.r.o (Amersfoort, The Netherlands). This commercial titania has been chosen since it is characterised by a very large surface area (217 $m^2 \cdot g^{-1}$) and it is in the anatase form, i.e., typically the most suitable titania crystalline phase for this photocatalytic application.

3.2. Synthesis of TiO_2

The precipitation method has been chosen to synthesise titania samples. In a typical synthesis, a 1.2 M titanyl sulphate solution and a 9.0 M NaOH solution are added dropwise and simultaneously to 200 mL of distilled water under vigorous stirring, in order to keep pH neutral. The $Ti(OH)_4$ suspension has been aged at 60 °C for 20 h. Afterwards, the precipitate has been filtered and washed with distilled water to remove sulphate ions. The absence of sulphates has been verified by means of a barium

chloride test [69]. Wet $Ti(OH)_4$ has been dried overnight at 110 °C and calcined at 400 °C for 4 h in air flow to obtain TiO_2.

3.3. Characterization of the Photocatalysts

XRD patterns have been collected on a Bruker D8 Advance powder diffractometer with a sealed X-ray tube (copper anode; operating conditions, 40 kV and 40 mA) and a Si(Li) solid state detector (Sol-X) set to discriminate the Cu Kα radiation. Apertures of divergence, receiving, and detector slits were 2.0 mm, 2.0 mm, and 0.2 mm, respectively. Data scans have been performed in the 2θ range of 5–75° with a 0.02° step size and counting times of 3 s/step. Quantitative phase analysis and crystallite size determination have been performed using the Rietveld method as implemented in the TOPAS v.4 program (Bruker AXS) using the fundamental parameters approach for line-profile fitting. The determination of the crystallite size was accomplished by the Double-Voigt approach and calculated as volume-weighted mean column heights based on integral breadths of peaks.

N_2 adsorption–desorption isotherms at 196 °C were performed using a MICROMERITICS ASAP 2000 analyser (Micromeritics Instruments Corporation, Norcross, GA, USA) to obtain information on the surface properties. All samples were previously outgassed at 200 °C for 2 h. The mesopore volume was measured as the adsorbed amount of N_2 after capillary condensation. The surface area was evaluated using the standard BET [70] equation and the pore size distribution was obtained using the BJH method applied to the isotherm desorption branch [71].

Diffuse reflectance spectroscopy (DRS) of carefully ground powders was performed with a Thermo Scientific Evolution 600 spectrophotometer, equipped with a diffuse reflectance accessory praying–mantis sampling kit (Harrick Scientific Products, NY, USA). A Spectralon1 disk was used as the reference material. The experimental absorption versus lambda plot was elaborated using the Kubelka–Munk function [72]. The band gap energy (Eg) of the catalysts are determined by the intercept of a linear fit to the absorption edge and they can be estimated using the standard equation, which is based on the relationship between frequency (c/λ) and photon energy ($Eg = 1240/\lambda$).

3.4. Photoactivity Tests in the Liquid Phase

Catalysts were suspended in water with a concentration of 0.3 $g \cdot L^{-1}$ at neutral pH. Na_2SO_3 (Sigma Aldrich, 98%) was used as a hole scavenger, with a concentration of 1.7 $g \cdot L^{-1}$. All these products were used without further purification. The gas phase was analysed by gas chromatography (Agilent, Santa Clara, CA, USA mod. 7890) equipped with a thermal conductivity detector (TCD) and a proper set up for the quantification of H_2, CH_4, CO, and polar/non-polar light gases. The liquid mixture has been analysed by means of a HPLC (Agilent 1220 Infinity) using a column (Alltech OA-10308, 300 mm_7.8 mm) with UV and refractive index (Agilent 1260 Infinity) detectors. Aqueous H_3PO_4 solution (0.1 wt %) was used as the eluent. The consumption of Na_2SO_3 was evaluated by iodometric titration. This method is based on the oxidation of sulphites (SO_3^{2-}) into sulphates (SO_4^{2-}) by iodine produced from a solution with a known concentration of potassium iodate (KIO_3, Sigma Aldrich, 98%) and potassium iodide (KI, Sigma Aldrich, 99%) in acid environment and the subsequent titration of the iodine excess with sodium thiosulphate ($Na_2S_2O_3$, Sigma Aldrich, 98%). The equivalence point of the titration was detected using starch solution as an indicator.

Photocatalytic reduction of CO_2 with H_2O was carried out at constant pressure of 7 bar, at a constant temperature of 80 °C for 24 h. The scheme of the experimental setup and details are shown elsewhere [30]. Briefly, it is an innovative pressurized batch photoreactor with a medium-pressure Hg lamp as the source of radiation. The emission range was between 254 nm and 364 nm. The lamp was cooled using an inner internal air flow of 2000 L h^{-1}. This air flow was selected to tune the average measured irradiance in the reactor to 50 W/m^2, for comparison with testing in the gas phase (vide infra). The emitted power was periodically measured by means of a photoradiometer (Delta OHM HD2102.2).

Before starting the irradiation of the reaction mixture the system was outgassed at constant CO_2 flow of 15 mL·min^{-1} at a pressure of 13 bar with the aim to eliminate air from the reactor head space. Then, in order to saturate water with CO_2, a static pressure of 7 bar of CO_2 was applied overnight.

3.5. Photoactivity Tests in the Vapour Phase

The catalytic apparatus was reported in a previous work [39]. CO_2 photoreduction was performed using a borate glass thin film reactor (length: 33 mm, height: 18 mm, thickness: 2 mm). Here the catalyst (10 mg) was inserted by depositing the catalyst suspended in 2-propanol on the light-exposed side of the reactor. Before tests, the catalyst was left overnight under helium flow to desorb all residual carbonaceous species.

The samples were illuminated using a 125 W mercury UVA lamp (purchased from Helios Italquartz s.r.l. with emission range 315–400 nm shielded by a special tubular quartz, to block radiations whose wavelength is lower than 350 nm), with an average irradiance of 50 W·m^{-2}, considering all emission wavelengths. Afterwards, a gaseous mixture of carbon dioxide and water has flowed through the reactor. Compressed CO_2 (99.99%) regulated by a mass flow controller was carried through a water bubbler kept at 40 °C to generate a CO_2 and H_2O vapour mixture (13.3 CO_2/H_2O molar ratio). The reactor was closed when the system reached the equilibrium state and this point was taken as the beginning of the reaction. Therefore, the reaction was not performed under a continuous gas flow, but it took place under static conditions. A total of 9.2 μmol of CO_2 and 0.7 μmol of H_2O were present within the sealed reactor. In all catalytic tests, the reaction time was 6 h.

The reaction products were analysed by a gas chromatograph (HP G1540A, Hewlett-Packard Company, Wilmington, DE, USA) equipped with a Porapak Q column and a TCD detector, appropriately calibrated to separate and quantify H_2, CH_4, and CO. Activity results are expressed in turn-over frequencies (TOFs) in μmol·gcat^{-1}·h^{-1}, as commonly used in the literature [42,73].

4. Conclusions

Breakthroughs in CO_2 photoreduction relies not only on the development of efficient photocatalysts, but also on finding the most suitable reaction conditions, and in particular reaction medium, which has never been investigated before. Throughout this work, it was shown that, to appreciate differences and effectiveness of photocatalytic materials, reaction conditions are not a trivial matter, but dramatically affect photocatalytic performances.

The choice of low-irradiance conditions allowed, on one side, to appreciate the differences in photocatalytic behaviour and, on the other, to minimise the energetic input.

Whatever the reaction conditions are, it was established that the crystal phase (i.e., anatase) and crystallinity increase titanium dioxide photoactivity, which excelled in lab-synthesised samples in comparison with commercial benchmark materials.

However, the choice of reaction medium dramatically drives the reaction pathway with consequences on process selectivity: vapour phase deoxygenation drives selectivity towards methane whereas, in the liquid phase, water dehydrogenation allows obtaining intermediate oxidation state products, i.e., formic acid, formaldehyde, and methanol.

Acknowledgments: The authors thank Tania Fantinel (Ca' Foscari University of Venice) for the excellent technical assistance. The financial support of Regione Veneto (project number: 2120-10-2121-2015) is gratefully acknowledged.

Author Contributions: All authors equally contributed to the preparation of this manuscript.

Conflicts of Interest: The authors declare no conflict of interest. The founding sponsors had no role in the design of the study; in the collection, analyses, or interpretation of data; in the writing of the manuscript; or in the decision to publish the results.

References

1. Dai, H.; Xie, X.; Xie, Y.; Liu, J.; Masui, T. Green growth: The economic impacts of large-scale renewable energy development in China. *Appl. Energy* **2016**, *162*, 435–449. [CrossRef]
2. Ghommem, M.; Haji, M.; Puri, I. Influence of natural and anthropogenic carbon dioxide sequestration on global warming. *Ecol. Model.* **2012**, *235–236*, 1–7. [CrossRef]
3. Framework Convention on Climate Change (FCCC). *Paris Agreement, Document FCCC/CP/2015/L.9/Rev.1*; FCCC: New York, NY, USA, 2015.
4. Nogia, P.; Sidhu, G.K.; Mehrotra, R.; Mehrotra, S. Capturing atmospheric carbon: Biological and nonbiological methods. *Int. J. Low-Carbon Technol.* **2016**, *11*, 266–274. [CrossRef]
5. Derevschikov, V.S.; Veselovskaya, J.V.; Kardash, T.Y.; Trubitsyn, D.A.; Okunev, A.G. Direct CO_2 capture from ambient air using K_2CO_3/Y_2O_3 composite sorbent. *Fuel* **2014**, *127*, 212–218. [CrossRef]
6. Alonso, A.; Moral-Vico, J.; Abo Markeb, A.; Busquets-Fité, M.; Komilis, D.; Puntes, V.; Sánchez, A.; Font, X. Critical review of existing nanomaterial adsorbents to capture carbon dioxide and methane. *Sci. Total Environ.* **2017**, *595*, 51–62. [CrossRef] [PubMed]
7. Holloway, S. Underground sequestration of carbon dioxide—A viable greenhouse gas mitigation option. *Energy* **2005**, *30*, 2318–2333. [CrossRef]
8. Koide, H.; Xue, Z. Carbon microbubbles sequestration: A novel technology for stable underground emplacement of greenhouse gases into wide variety of saline aquifers, fractured rocks and tight reservoirs. *Energy Procedia* **2009**, *1*, 3655–3662. [CrossRef]
9. Raza, A.; Gholami, R.; Rezaee, R.; Han Bing, C.; Nagarajan, R.; Ali Hamid, M. Assessment of CO_2 residual trapping in depleted reservoirs used for geosequestration. *J. Nat. Gas Sci. Eng.* **2017**, *43*, 137–155. [CrossRef]
10. Cuéllar-Franca, R.M.; Azapagic, A. Carbon capture, storage and utilisation technologies: A critical analysis and comparison of their life cycle environmental impacts. *J. CO_2 Util.* **2015**, *9*, 82–102. [CrossRef]
11. Asahi, R.; Morikawa, T.; Irie, H.; Ohwaki, T. Nitrogen-doped titanium dioxide as visible-light-sensitive photocatalyst: designs, developments, and prospects. *Chem. Rev.* **2014**, *114*, 9824–9852. [CrossRef] [PubMed]
12. Meylan, F.; Moreau, V.; Erkman, S. CO_2 utilization in the perspective of industrial ecology, an overview. *J. CO_2 Util.* **2015**, *12*, 2–9. [CrossRef]
13. Narayanan, H.; Viswanathan, B.; Yesodharan, S. Photocatalytic reduction of carbon dioxide: Issues and prospects. *Curr. Catal.* **2016**, *5*, 79–107. [CrossRef]
14. Kočí, K.; Obalová, L.; Lacný, Z. Photocatalytic reduction of CO_2 over TiO_2 based catalysts. *Chem. Pap.* **2008**, *62*, 1–9. [CrossRef]
15. Varghese, O.K.; Paulose, M.; LaTempa, T.J.; Grimes, C. High-rate solar photocatalytic conversion of CO_2 and water vapor to hydrocarbon fuels. *Nano Lett.* **2009**, *9*, 731–737. [CrossRef] [PubMed]
16. Sastre, F.; Puga, A.V.; Liu, L.; Corma, A.; García, H. Complete photocatalytic reduction of CO_2 to methane by H_2 under solar light irradiation. *J. Am. Chem. Soc.* **2014**, *136*, 6798–6801. [CrossRef] [PubMed]
17. Kohno, Y.; Tanaka, T.; Funabiki, T.; Yoshida, S. Reaction mechanism in the photoreduction of CO_2 with CH_4 over ZrO_2. *Phys. Chem. Chem. Phys.* **2000**, *2*, 5302–5307. [CrossRef]
18. Habisreutinger, S.N.; Schmidt-Mende, L.; Stolarczyk, J.K. Photocatalytic reduction of CO_2 on TiO_2 and other semiconductors. *Angew. Chem. Int. Ed.* **2013**, *52*, 7372–7408. [CrossRef] [PubMed]
19. Nikokavoura, A.; Trapalis, C. Alternative photocatalysts to TiO_2 for the photocatalytic reduction of CO_2. *Appl. Surf. Sci.* **2017**, *391*, 149–174. [CrossRef]
20. Wang, S.; Wang, X. Photocatalytic CO_2 reduction by CdS promoted with a zeolitic imidazolate framework. *Appl. Catal. B Environ.* **2015**, *162*, 494–500. [CrossRef]
21. Liu, G.; Hoivik, N.; Wang, K.; Jakobsen, H. Engineering TiO_2 nanomaterials for CO_2 conversion/solar fuels. *Sol. Energy Mater. Sol. Cells* **2012**, *105*, 53–68. [CrossRef]
22. Mori, K.; Yamashita, H.; Anpo, M. Photocatalytic reduction of CO_2 with H_2O on various titanium oxide photocatalysts. *RSC Adv.* **2012**, *2*, 3165–3172. [CrossRef]
23. Inoue, T.; Fujishima, A.; Konishi, S.; Honda, K. Photoelectrocatalytic reduction of carbon dioxide in aqueous suspensions of semiconductor powders. *Nature* **1979**, *277*, 637–638. [CrossRef]
24. Anpo, M.; Yamashita, H.; Ikeue, K.; Fujii, Y.; Zhang, S.G.; Ichihashi, Y.; Park, D.R.; Suzuki, Y.; Koyano, K.; Tatsumi, T. Photocatalytic reduction of CO_2 with H_2O on Ti-MCM-41 and Ti-MCM-48 mesoporous zeolite catalysts. *Catal. Today* **1998**, *44*, 327–331. [CrossRef]

25. Richardson, P.L.; Perdigoto, M.L.N.; Wang, W.; Lopes, R.J.G. Heterogeneous photo-enhanced conversion of carbon dioxide to formic acid with copper- and gallium-doped titania nanocomposites. *Appl. Catal. B Environ.* **2013**, *132–133*, 408–415. [CrossRef]
26. Ulagappan, N.; Frei, H. Mechanistic Study of CO_2 Photoreduction in Ti Silicalite Molecular Sieve by FT-IR Spectroscopy. *J. Phys. Chem.* **2000**, *104*, 7834–7839. [CrossRef]
27. Liu, B.; Torimoto, T.; Matsumoto, H.; Yoneyama, H. Effect of solvents on photocatalytic reduction of carbon dioxide using TiO_2 nanocrystal photocatalyst embedded in SiO_2 matrices. *J. Photochem. Photobiol. A Chem.* **1997**, *108*, 187–192. [CrossRef]
28. Ampelli, C.; Centi, G.; Passalacqua, R.; Perathoner, S. Synthesis of solar fuels by a novel photoelectrocatalytic approach. *Energy Environ. Sci.* **2010**, *3*, 292–301. [CrossRef]
29. Zhao, Z.; Fan, J.; Xie, M.; Wang, Z. Photo-catalytic reduction of carbon dioxide with in-situ synthesized CoPc/TiO_2 under visible light irradiation. *J. Clean. Prod.* **2009**, *17*, 1025–1029. [CrossRef]
30. Reli, M.; Šihor, M.; Kočí, K.; Praus, P.; Kozák, O.; Obalová, L. Influence of reaction medium on CO_2 photocatalytic reduction yields over Zns-MMT. *GeoSci. Eng.* **2012**, *58*, 34–42. [CrossRef]
31. Dodds, W.S.; Stutzman, L.F.; Sollami, B.J. Carbon dioxide solubility in water. *Ind. Eng. Chem. Chem. Eng. Data Ser.* **1956**, *1*, 92–95. [CrossRef]
32. Rossetti, I.; Villa, A.; Compagnoni, M.; Prati, L.; Ramis, G.; Pirola, C.; Bianchi, C.L.; Wang, W.; Wang, D. CO_2 photoconversion to fuels under high pressure: Effect of TiO_2 phase and of unconventional reaction conditions. *Catal. Sci. Technol.* **2015**, *5*, 4481–4487. [CrossRef]
33. Nguyen, T.; Wu, J. Photoreduction of CO_2 to fuels under sunlight using optical-fiber reactor. *Sol. Energy Mater. Sol. Cells* **2008**, *92*, 864–872. [CrossRef]
34. Li, Y.; Wang, W.N.; Zhan, Z.L.; Woo, M.H.; Wu, C.Y.; Biswas, P. Photocatalytic reduction of CO_2 with H_2O on mesoporous silica supported Cu/TiO_2 catalysts. *Appl. Catal. B Environ.* **2010**, *100*, 386–392. [CrossRef]
35. Wang, W.N.; An, W.J.; Ramalingam, B.; Mukherjee, S.; Niedzwiedzki, D.M.; Gangopadhyay, S.; Biswas, P. Size and structure matter: enhanced CO_2 photoreduction efficiency by size-resolved ultrafine Pt nanoparticles on TiO_2 single crystals. *J. Am. Chem. Soc.* **2012**, *134*, 11276–11281. [CrossRef] [PubMed]
36. Ola, O.; Maroto-Valer, M. Role of catalyst carriers in CO_2 photoreduction over nanocrystalline nickel loaded TiO_2-based photocatalysts. *J. Catal.* **2014**, *309*, 300–308. [CrossRef]
37. Tahir, M.; Amin, N. Indium-doped TiO_2 nanoparticles for photocatalytic CO_2 reduction with H_2O vapors to CH_4. *Appl. Catal. B Environ.* **2015**, *162*, 98–109. [CrossRef]
38. Michalkiewicz, B.; Majewska, J.; Kądziołka, G.; Bubacz, K.; Mozia, S.; Morawski, A.W. Reduction of CO_2 by adsorption and reaction on surface of TiO_2-nitrogen modified photocatalyst. *J. CO_2 Util.* **2014**, *5*, 47–52. [CrossRef]
39. Olivo, A.; Trevisan, V.; Ghedini, E.; Pinna, F.; Bianchi, C.L.; Naldoni, A.; Cruciani, G.; Signoretto, M. CO_2 photoreduction with water: Catalyst and process investigation. *J. CO_2 Util.* **2015**, *12*, 86–94. [CrossRef]
40. Bideau-Mehu, A.; Guern, Y.; Abjean, R.; Johannin-Gilles, A. Interferometric determination of the refractive index of carbon dioxide in the ultraviolet region. *Opt. Commun.* **1973**, *9*, 432–434. [CrossRef]
41. Lide, D.R. *CRC Handbook of Chemistry and Physics*, 89th ed.; CRC Press: Boca Raton, FL, USA, 2005; pp. 4–140.
42. Anpo, M.; Yamashita, H.; Ichihashi, Y.; Ehara, S. Photocatalytic reduction of CO_2 with H_2O on various titanium oxide catalysts. *J. Electroanal. Chem.* **1995**, *396*, 21–26. [CrossRef]
43. Zhang, Q.; Gao, T.; Andino, J.M.; Li, Y. Copper and iodine co-modified TiO_2 nanoparticles for improved activity of CO_2 photoreduction with water vapor. *Appl. Catal. B Environ.* **2012**, *123–124*, 257–267. [CrossRef]
44. Tahir, M.; Amin, N.S. Photocatalytic reduction of carbon dioxide with water vapors over montmorillonite modified TiO_2 nanocomposites. *Appl. Catal. B Environ.* **2013**, *142–143*, 512–522. [CrossRef]
45. Matějová, L.; Kočí, K.; Reli, M.; Čapek, L.; Hospodková, A.; Peikertová, P.; Matěj, Z.; Obalová, L.; Wach, A.; Kuśtrowski, P.; et al. Preparation, characterization and photocatalytic properties of cerium doped TiO_2: On the effect of Ce loading on the photocatalytic reduction of carbon dioxide. *Appl. Catal. B Environ.* **2014**, *152–153*, 172–183. [CrossRef]
46. Ikeue, K.; Yamashita, H.; Anpo, M. Photocatalytic Reduction of CO_2 with H_2O on Ti−β Zeolite Photocatalysts: Effect of the hydrophobic and hydrophilic properties. *J. Phys. Chem. B* **2001**, *105*, 8350–8355. [CrossRef]
47. Wu, J.C.S.; Lin, H.M.; Lai, C.L. Photo reduction of CO_2 to methanol using optical-fiber photoreactor. *Appl. Catal. A Gen.* **2005**, *296*, 194–200. [CrossRef]

48. Vijayan, B.; Dimitrijevic, N.M.; Rajh, T.; Gray, K. Effect of calcination temperature on the photocatalytic reduction and oxidation processes of hydrothermally synthesized titania nanotubes. *J. Phys. Chem. C* **2010**, *114*, 12994–13002. [CrossRef]
49. Woolerton, T.W.; Sheard, S.; Reisner, E.; Pierce, E.; Ragsdale, S.W.; Armstrong, F.A. Efficient and clean photoreduction of CO_2 to CO by enzyme-modified TiO_2 nanoparticles using visible light. *J. Am. Chem. Soc.* **2010**, *132*, 2132–2133. [CrossRef] [PubMed]
50. Tahir, M.; Tahir, B.; Amin, N. Synergistic effect in plasmonic Au/Ag alloy NPs co-coated TiO_2 NWs toward visible-light enhanced CO_2 photoreduction to fuels. *Appl. Catal. B Environ.* **2017**, *204*, 548–560. [CrossRef]
51. Jitputti, J.; Suzuki, Y.; Yoshikawa, S. Synthesis of TiO_2 nanowires and their photocatalytic activity for hydrogen evolution. *Catal. Commun.* **2008**, *9*, 1265–1271. [CrossRef]
52. Bagheri, S.; Hir, Z.A.M.; Yousefi, A.T.; Bee, S.; Hamid, A. Progress on mesoporous titanium dioxide: Synthesis, modification and applications. *Microporous Mesoporous Mater.* **2014**, *218*, 206–222. [CrossRef]
53. Di Paola, A.; Bellardita, M.; Palmisano, L. Brookite, the least known TiO_2 photocatalyst. *Catalysts* **2013**, *3*, 36–73. [CrossRef]
54. Ola, O.; Maroto-Valer, M. Review of material design and reactor engineering on TiO_2 photocatalysis for CO_2 reduction. *J. Photochem. Photobiol. C* **2015**, *24*, 16–42. [CrossRef]
55. Bellardita, M.; Di Paola, A.; Garcia-Lopez, E.; Loddo, V.; Marcì, G.; Palmisano, L. Photocatalytic CO_2 reduction in gas-solid regime in the presence of bare, SiO_2 supported or Cu-loaded TiO_2 samples. *Curr. Org. Chem.* **2013**, *17*, 2440–2448. [CrossRef]
56. Titanium Dioxide for Catalysts and Supports. Available online: http://www.eurosupport.nl/pdf/catalytic_titanias.pdf (accessed on 22 August 2017).
57. Ding, Z.; Lu, G.Q.; Greenfield, P.F. Role of the crystallite phase of tio_2 in heterogeneous photocatalysis for phenol oxidation in water. *J. Phys. Chem. B* **2000**, *104*, 4815–4820. [CrossRef]
58. Hurum, D.C.; Agrios, A.G.; Gray, K.A.; Rajh, T.; Thurnauer, M.C. Explaining the enhanced photocatalytic activity of Degussa P25 mixed-phase TiO_2 using EPR. *J. Phys. Chem. B* **2003**, *107*, 4545–4549. [CrossRef]
59. Carini, G., Jr.; Parrino, F.; Palmisano, G.; Scandura, G.; Citro, I.; Calogero, G.; Bartolotta, A.; Di Marco, G. Nanostructured anatase TiO_2 densified at high pressure as advanced visible light photocatalysts. *Photochem. Photobiol. Sci.* **2015**, *14*, 1685–1693. [CrossRef] [PubMed]
60. Grigioni, I.; Dozzi, M.V.; Bernareggi, M.; Chiarello, G.L.; Selli, E. Photocatalytic CO_2 reduction vs. H_2 production: The effects of surface carbon-containing impurities on the performance of TiO_2-based photocatalysts. *Catal. Today* **2017**, *281*, 214–220. [CrossRef]
61. Karamian, E.; Sharafina, S. On the general mechanism of photocatalytic reduction of CO_2. *J. CO_2 Util.* **2016**, *16*, 194–203. [CrossRef]
62. Liu, L. Understanding the reaction mechanism of photocatalytic reduction of CO_2 with H_2O on TiO_2-based photocatalysts: A review. *Aerosol Air Qual. Res.* **2014**, *2*, 453–469. [CrossRef]
63. Tan, S.; Zou, L.; Hu, E. Photocatalytic reduction of carbon dioxide into gaseous hydrocarbon using TiO_2 pellets. *Catal. Today* **2006**, *115*, 269–273. [CrossRef]
64. Galli, F.; Compagnoni, M.; Vitali, D.; Pirola, C.; Bianchi, C.L.; Villa, A.; Prati, L.; Rossetti, I. CO_2 photoreduction at high pressure to both gas and liquid products over titanium dioxide. *Appl. Catal. B Environ.* **2017**, *200*, 386–391. [CrossRef]
65. Baran, T.; Wojtyła, S.; Dibenedetto, A.; Aresta, M.; Macyk, W. Zinc sulfide functionalized with ruthenium nanoparticles for photocatalytic reduction of CO_2. *Appl. Catal. B Environ.* **2015**, *178*, 170–176. [CrossRef]
66. Kočí, K.; Obalová, L.; Matějová, L.; Plachá, D.; Lacný, Z.; Jirkovský, J.; Šolková, O. Effect of TiO_2 particle size on the photocatalytic reduction of CO_2. *Appl. Catal. B Environ.* **2009**, *89*, 494–502. [CrossRef]
67. Chen, X.; Shen, S.; Guo, L.; Mao, S.S. Semiconductor-based photocatalytic hydrogen generation. *Chem. Rev.* **2010**, *110*, 6503–6570. [CrossRef] [PubMed]
68. Matějová, L.; Šihor, M.; Lang, J.; Troppová, I.; Ambrožová, N.; Reli, M.; Brunátová, T.; Čapek, L.; Kotarba, A.; Kočí, K. Investigation of low Ce amount doped-TiO_2 prepared by using pressurized fluids in photocatalytic N_2O decomposition and CO_2 reduction. *J. Sol-Gel Sci. Technol.* **2017**, in press. [CrossRef]
69. Tabatabai, M.A. A rapid method for determination of sulfate in water samples. *Environ. Lett.* **1974**, *7*, 237–243. [CrossRef]
70. Brunauer, S.; Emmett, P.H.; Teller, E. Adsorption of gases in multimolecular layers. *J. Am. Chem. Soc.* **1938**, *60*, 309–319. [CrossRef]

71. Barrett, E.P.; Joyner, L.S.; Halenda, P.P. The determination of pore volume and area distributions in porous substances. I. Computations from nitrogen isotherms. *J. Am. Chem. Soc.* **1951**, *73*, 373–380. [CrossRef]
72. Kubelka, P.; Munk, F. Ein beitrag zur optik der farbanstriche. *Z. Phys.* **1931**, *12*, 593–601.
73. Liu, D.; Fernandez, Y.; Ola, O.; Maroto-Valer, M.; Parlett, C.M.A.; Lee, A.F.; Wu, J.C.S. On the impact of Cu dispersion on CO_2 photoreduction over Cu/TiO_2. *Catal. Commun.* **2012**, *25*, 78–82. [CrossRef]